824. Numerical model of journal bearing lubrication considering a bending stiffness effect

Juhwan Choi[1], Seong Su Kim[2], Sungsoo Rhim[3], Jin Hwan Choi[4]
[1, 2]R&D Center, Function Bay, Inc., Gyeonggi-do, 463-400, South Korea
[3, 4]Department of Mechanical Engineering, Kyung Hee University, Gyeonggi-do, 446-701, South Korea
E-mail: [1]*juhwan@functionbay.co.kr*, [2]*seongsu@functionbay.co.kr*, [3]*ssrhim@khu.ac.kr*, [4]*jhchoi@khu.ac.kr*

(Received 30 July 2012; accepted 4 September 2012)

Abstract. An analysis for operating characteristics of journal bearing lubrication system is performed based on the numerical model. Dynamic bearing lubrication characteristics such as oil film pressure and thickness distribution can be analyzed through a numerical model with an integration of elastohydrodynamics and multi-flexible-body dynamics (MFBD). In particular, the oil film thickness variation by elastic deformation is considered in the elastohydrodynamic analysis by applying the bending stiffness effect of journal. And the oil film thickness variation by the bending stiffness effect is applied to the fluid governing equations to calculate the oil film pressure in the elastohydrodynamic lubrication region. A series of process proposed in this study is available for the analysis of realistic elastohydrodynamic lubrication phenomenon. Also, a numerical example for the journal bearing lubrication system is demonstrated and compared with the experimental results. The numerical results considering the bending stiffness effect show a good agreement with the experimental results.

Keywords: journal bearing, lubrication, elastohydrodynamics, MFBD, bending stiffness effect.

1. Introduction

The journal bearings, which is the one of the widely used machine elements, transmit the power while reducing the friction and resisting the external loads. In particular, in the internal combustion engine which is frequently used for power generation, the various journal bearings are used between the piston, piston pin, connecting rod, crankshaft, and engine block. These journal bearings, which are under the alternating loads caused by the gas forces of the internal engines, guarantee the smooth operation of the engine and are tightly related to the durability of the engine system. In order to achieve the high-performance output and to reduce the engine weight, the importance of the bearing lubrication analysis has been increased [1-3].

The study of bearing lubrication is based on the Reynolds equation [4] which describes the thickness and pressure of fluid film generated by the relative motion of objects. Accordingly, to estimate the lubrication film characteristics such as the oil film thickness and pressure, a multi-flexible-body dynamics analysis (MFBD) [5-7] is needed to obtain the information for the relative motion between journal and bearing and the elastohydrodynamic lubrication analysis is also needed to get lubrication characteristics.

Generally, elastohydrodynamic lubrication can be classified by two types based on the relationship between surface roughness and oil film thickness. One type is the full-film lubrication. It has been widely used when the lubricant film is sufficiently thick in which there is no significant asperity contact. In this case, the pressure is only governed by Reynolds equation which is first established by Reynolds [4]. The other type is the mixed lubrication. When the lubricant film is not enough to thick, the asperity contacts between two bodies can occur [8, 9]. Therefore, in mixed lubrication region, the total pressure should be treated as the sum of the pressure induced by the fluid flow and the asperity contact. This study uses the Reynolds equation to obtain the hydrodynamic pressure and Greenwood and Tripp's asperity contact model [9] to obtain asperity contact pressure.

To obtain more reasonable results for lubrication characteristics, it is also important to consider the variation for oil film thickness and oil film pressure resulting from the elastic

deformation of flexible bodies. To consider this effect on the elastohydrodynamic analysis, this study proposes a numerical model which can express the bending effect of journal in the journal bearing system. The proposed bending effect is based on the beam theory.

In the Section 2 and 3, the MFBD and EHD theories are briefly introduced, respectively. The numerical model considering the bending effect of journal is introduced in Section 4. Numerical analysis procedure is explained in Section 5. A numerical example is discussed in Section 6 and the conclusions are in Section 7.

2. Multi-Flexible-Body Dynamics

In this section, the brief formulations for MBD and MFBD are introduced. The detailed information is described well in [7].

2. 1 MBD Formulation

The coordinate systems for two contiguous rigid bodies in 3D space are shown in Fig. 1. Two rigid bodies are connected by a joint, and an external force $\mathbf{F}$ is acting on the rigid body j. The X-Y-Z frame is global reference frame and x'-y'-z' is body reference frame with respect to the X-Y-Z frame. The subscript i means the inboard body of body j in the spanning tree of a recursive formulation.

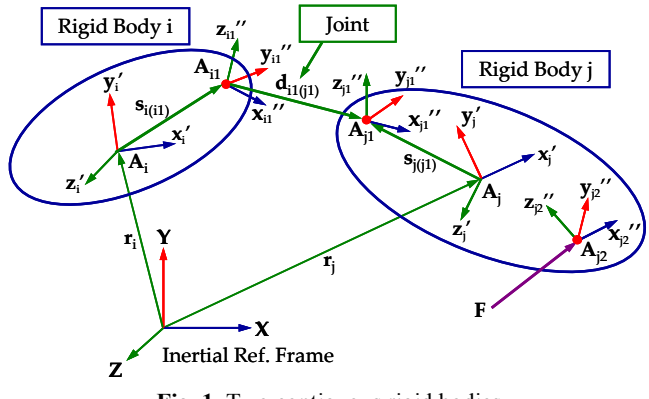

Fig. 1. Two contiguous rigid bodies

The equations of motion for a constrained mechanical system in the joint space have been obtained by using the velocity transformation method as follows:

$$\mathbf{F} = \mathbf{B}^{\mathrm{T}} (\mathbf{M}\dot{\mathbf{Y}} + \mathbf{\Phi}_{\mathbf{Z}}^{\mathrm{T}}\boldsymbol{\lambda} - \mathbf{Q}) = \mathbf{0} \quad (1)$$

where $\mathbf{\Phi}$ and $\boldsymbol{\lambda}$, respectively, denote the cut joint constraint and the corresponding Lagrange multiplier. $\mathbf{M}$ is a mass matrix, $\mathbf{Y}$ is a Cartesian velocity vector and $\mathbf{Q}$ is a force vector including the external forces in the Cartesian space. And $\mathbf{B}$ is a velocity transformation matrix between the relative space and Cartesian space.

2. 2 MFBD Formulation

The equation of motion for the rigid body can be expanded from the Eq. (1) as follows:

$$\mathbf{F}^{r} = \mathbf{B}^{\mathrm{T}} \left(\mathbf{M}^{r}\dot{\mathbf{Y}}^{r} + \mathbf{\Phi}_{\mathbf{z}}^{rr\mathrm{T}}\boldsymbol{\lambda}^{rr} + \mathbf{\Phi}_{\mathbf{z}}^{er\mathrm{T}}\boldsymbol{\lambda}^{er} - \mathbf{Q}^{r} \right) = \mathbf{0} \quad (2)$$

where the superscript *r* denotes a rigid body quantity. The superscripts *rr* means the quantities between rigid bodies and the superscript *er* means the quantities between a flexible body node and a rigid body. The constraints equations between rigid bodies are expressed as a function of the rigid body generalized coordinates $\mathbf{q}^r$ as follows:

$$\mathbf{\Phi}^{rr} = \mathbf{\Phi}^{rr}\left(\mathbf{q}^r, t\right) \tag{3}$$

Similarly, we can derive the equations of motion for the flexible body as follows:

$$\mathbf{F}^e = \mathbf{M}^e\ddot{\mathbf{q}}^e + \mathbf{\Phi}_{\mathbf{q}^e}^{ee\,\mathrm{T}}\boldsymbol{\lambda}^{ee} + \mathbf{\Phi}_{\mathbf{q}^e}^{er\,\mathrm{T}}\boldsymbol{\lambda}^{er} - \mathbf{Q}^e = \mathbf{0} \tag{4}$$

where the superscript *e* denotes a quantity describing a flexible body node and $\mathbf{q}^e$ is the generalized coordinate for the flexible body nodes. The superscript *ee* represents a relative quantity between a flexible body nodes and the superscript *er* denotes a relative quantity between a flexible body node and a rigid body. The forces $\mathbf{Q}^e$ between flexible body nodes can be expressed as the sum of the element forces and applied forces such as gravity or contact forces. The flexible body joint constraints $\mathbf{\Phi}^{er}$ between a flexible body node and a virtual rigid body can be expressed as follows:

$$\mathbf{\Phi}^{er} = \mathbf{\Phi}^{er}\left(\mathbf{q}^e, \mathbf{q}^r, t\right) \tag{5}$$

Similarly, the constraint equations $\mathbf{\Phi}^{ee}$ between flexible body nodes can be expressed as Eq. (6):

$$\mathbf{\Phi}^{ee} = \mathbf{\Phi}^{ee}\left(\mathbf{q}^e, t\right) \tag{6}$$

Finally, we can compose the whole system matrix for the MFBD problems as shown in Eq. (7) and we can solve Eq. (7) using a sparse linear solver to find the incremental quantities, which are added to the previous solution. This study used a generalized-alpha method for time integration [10]:

$$\begin{bmatrix} \dfrac{\partial \mathbf{F}^e}{\partial \mathbf{q}^e} & \mathbf{\Phi}_{\mathbf{q}^e}^{ee\,\mathrm{T}} & \dfrac{\partial \mathbf{F}^e}{\partial \mathbf{q}^r} & \mathbf{0} & \mathbf{\Phi}_{\mathbf{q}^e}^{er\,\mathrm{T}} \\ \mathbf{\Phi}_{\mathbf{q}^e}^{ee} & \mathbf{0} & \mathbf{0} & \mathbf{0} & \mathbf{0} \\ \dfrac{\partial \mathbf{F}^r}{\partial \mathbf{q}^e} & \mathbf{0} & \dfrac{\partial \mathbf{F}^r}{\partial \mathbf{q}^r} & \mathbf{B}^{\mathrm{T}}\mathbf{\Phi}_{\mathbf{z}}^{rr\,\mathrm{T}} & \mathbf{B}^{\mathrm{T}}\mathbf{\Phi}_{\mathbf{z}}^{er\,\mathrm{T}} \\ \mathbf{0} & \mathbf{0} & \mathbf{\Phi}_{\mathbf{q}^r}^{rr} & \mathbf{0} & \mathbf{0} \\ \mathbf{\Phi}_{\mathbf{q}^e}^{er} & \mathbf{0} & \mathbf{\Phi}_{\mathbf{q}^r}^{er} & \mathbf{0} & \mathbf{0} \end{bmatrix} \begin{bmatrix} \Delta\mathbf{q}^{ee} \\ \Delta\boldsymbol{\lambda}^{ee} \\ \Delta\mathbf{q}^{rr} \\ \Delta\boldsymbol{\lambda}^{rr} \\ \Delta\boldsymbol{\lambda}^{er} \end{bmatrix} = -\begin{bmatrix} \mathbf{F}^e \\ \mathbf{\Phi}^{ee} \\ \mathbf{F}^r \\ \mathbf{\Phi}^{rr} \\ \mathbf{\Phi}^{er} \end{bmatrix} \tag{7}$$

3. Elastohydrodynamics (EHD)

3. 1 Governing Equation of Hydrodynamics

Fig. 2 shows a schematic diagram for relative motion and dimensions between a bearing and a journal. In the figure, R is the journal radius and C_r is the clearance in the journal bearing lubrication problems.

The governing equation for the fluid flow becomes the Couette-Poiseuille flow equation [11-13]. Then, if the mass or flow rate conservation law is applied, the Reynolds' equation for the hydrodynamic problems can be expressed as Eq. (8):

$$\frac{\partial}{\partial x}\left(\Gamma\frac{\partial p}{\partial x}\right) + \frac{\partial}{\partial z}\left(\Gamma\frac{\partial p}{\partial z}\right) = 12V + 6U\frac{\partial H}{\partial x} + 6W\frac{\partial H}{\partial z}, \quad \Gamma = \frac{H^3}{\mu} \tag{8}$$

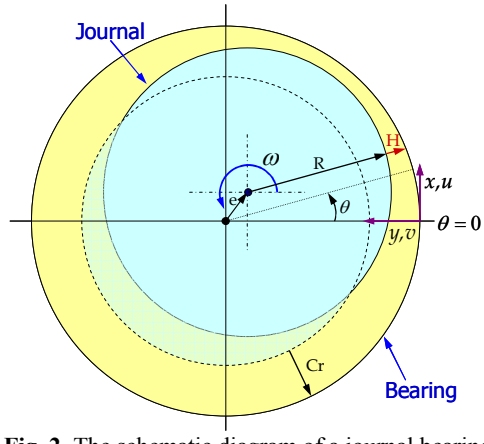

Fig. 2. The schematic diagram of a journal bearing

Here U, V and W are x, y and z components of the relative velocity of the journal surface (at $y = H$), respectively, with respect to the bearing. H is the oil film thickness considering the bending effect and μ is the dynamic viscosity. The Eq. (8) is solved iteratively with the successive over-relaxation method [14]. The oil film thickness without bending effect is defined as Eq. (9):

$$H_0(\theta) = C_r - e_x \cos\theta - e_y \sin\theta \tag{9}$$

Additionally, to support the general-purpose EHD solution, groove and oil hole effects are also implemented as the pressure boundary conditions.

3. 2 Asperity Contact

When the oil film thickness is not enough thick compared to the surface roughness, the contact pressure resulting from the asperities between bodies should be considered as shown in Fig. 3.

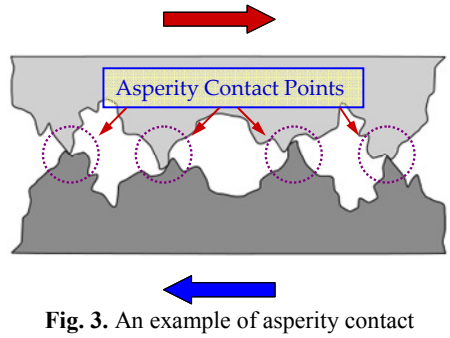

Fig. 3. An example of asperity contact

The asperity contact model by [9] is used to model the mixed lubrication region. In Greenwood and Tripp's model, the asperity contact pressure p_a can be calculated as follows:

$$p_a(H) = KE' F_{5/2}(H/\sigma_s)$$

$$F_{5/2}\left(\frac{H}{\sigma_s}\right) = \begin{cases} 4.4086\times10^{-5}\left(4-\dfrac{H}{\sigma_s}\right)^{6.804}, & \text{if } \dfrac{H}{\sigma_s} < 4 \\ 0, & \text{otherwise} \end{cases} \tag{10}$$

where K is the elastic factor and σ_s is the root mean square of the asperity summit heights and E' is the composite elastic modulus [15].

4. Bending Stiffness Effect

4. 1 Bending Effect of Journal

When a high external load is applied to the journal bearing, the journal can be bent and the variation of gap δ between journal and bearing occurs in axial direction as shown in Fig. 4. Because this gap is related to the oil film thickness, we need to consider this gap for the oil film thickness evaluation to analyze more accurate lubrication characteristics. The oil film thickness considering the bending of journal can be defined as follows:

$$H(\theta) = H_0(\theta) - \delta_x \cos\theta - \delta_y \cos\theta \tag{11}$$

where H_0 is defined in Eq. (9) and H is used to solve Reynolds equation of Eq. (8). In this study, the bending stiffness effect model based on the beam theory is proposed to obtain the gap δ.

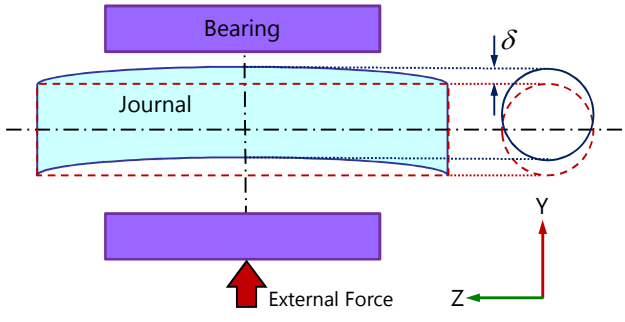

Fig. 4. Bending phenomenon of journal

4. 2. Bending Stiffness Effect Model

To express the bending phenomenon of journal, two dimensional beam model is introduced as shown in Fig. 5. In this numerical model, translational and rotational springs are used to adjust the degree of restriction for both ends of beam. If the spring coefficients for translational and rotational spring are infinite, both ends of beam can be regarded as fixed. Additionally, pressure applied to journal is assumed as a line distributed load for beam.

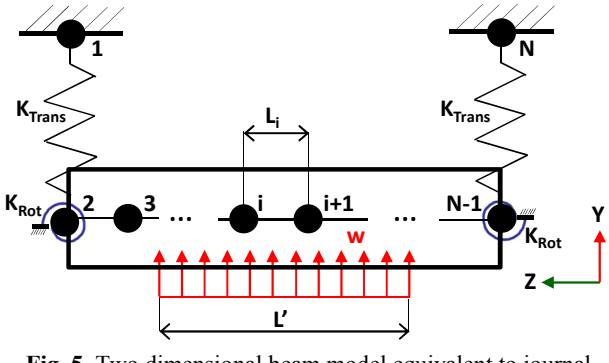

Fig. 5. Two dimensional beam model equivalent to journal

Based on above mentioned features, we can make a general beam model which has N nodes and $N-1$ elements. In accordance with the beam theory, stiffness matrix for each element except for elements at both ends is defined as follows:

$$\mathbf{K}_i = EI\begin{bmatrix} \frac{12}{L_i^3} & \frac{6}{L_i^2} & \frac{-12}{L_i^3} & \frac{6}{L_i^2} \\ \frac{6}{L_i^2} & \frac{4}{L_i} & \frac{-6}{L_i^2} & \frac{2}{L_i} \\ \frac{-12}{L_i^3} & \frac{-6}{L_i^2} & \frac{12}{L_i^3} & \frac{-6}{L_i^2} \\ \frac{6}{L_i^2} & \frac{2}{L_i} & \frac{-6}{L_i^2} & \frac{4}{L_i} \end{bmatrix}, \text{ for } 2 \le i \le N-2 \tag{12}$$

where $\mathbf{K}_i$ and L_i denotes the stiffness matrix and the length of i-th element except for elements at both ends, respectively. E is the Young's modulus and I is the area moment of inertia of journal body. For the both end elements, stiffness matrix is defined as follows:

$$\mathbf{K}_i = \begin{bmatrix} K_{Trans} & 0 & -K_{Trans} & 0 \\ 0 & K_{Rot} & 0 & -K_{Rot} \\ -K_{Trans} & 0 & K_{Trans} & 0 \\ 0 & -K_{Rot} & 0 & K_{Rot} \end{bmatrix}, \text{ for } i = 1 \text{ and } N-1 \tag{13}$$

where K_{Trans} and K_{Rot} are translational and rotational spring coefficient, respectively. Line distributed load w can be calculated as follows:

$$w = \frac{F}{L'} \tag{14}$$

where F is the external force applied to journal resulting from the oil film pressure and L' is the length of part in which oil film pressure occurs.

Accordingly, if a line distributed load is applied on i-th element, the force vector of i-th element can be defined as follows:

$$\mathbf{f}_i = \begin{bmatrix} \frac{wL_i}{2} & \frac{wL_i^2}{12} & \frac{wL_i}{2} & -\frac{wL_i^2}{12} \end{bmatrix}^T \tag{15}$$

Once we define the stiffness matrix and force vector for the all elements, we can create a global stiffness matrix and force vector by superposing the element stiffness matrix and force vector as follows:

$$\mathbf{f} = \mathbf{K}\boldsymbol{\delta} \tag{16}$$

where $\mathbf{K}$ is a global stiffness matrix and $\mathbf{f}$ is a global force vector. $\boldsymbol{\delta}$ denotes the normal and rotational displacement vector for all nodes. If we get the displacement vector $\boldsymbol{\delta}$ for all nodes by solving Eq. (16), the gap δ mentioned in Section 4.1 can be evaluated.

5. Numerical Analysis Procedure

In this study, EHD and MFBD solvers are used together to analyze the fluid lubrication and flexible multibody dynamic characteristics of the journal bearing.

In EHD solver, pressure distributions are calculated by considering the bending stiffness effect of the journal. First, the relative velocity of the journal surface with respect to the bearing and oil film thickness is calculated over the EHD grid points using the information for the positions and velocities of journal and bearing. Additionally, oil film thickness that is calculated previously is updated by considering the variation of oil film thickness resulting from the bending of the journal. Finally, Reynolds equation is solved with the asperity contact force for

the given boundary conditions. And then, the calculated pressure field and the resulting force and torque are transmitted to the MFBD solver.

In the MFBD solver, the transmitted force and torque data are used as the external forces or torques acting on the journal and bearing. Then, from the MFBD analysis, positions and velocities of journal and bearing are calculated. These data are transmitted to the EHD solver again. Fig. 6 shows the procedure of the fluid-structure interaction solving method between EHD and MFBD solvers.

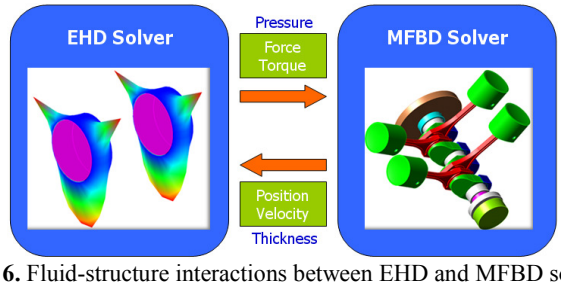

Fig. 6. Fluid-structure interactions between EHD and MFBD solver

6. Numerical Example

To implement the EHD module considering the bending stiffness effect with MFBD solver together, this study used the RecurDyn^{TM} [16] MFBD environment. To validate the numerical results of this study, the experimental results of Okamoto et al. [17] are used. The detailed explanation about the numerical model is described well in [17]. Fig. 7 shows the numerical model and measured points of the oil film pressure. The rotational speed of shaft is 3250 rpm.

Table 1. The parameters of numerical model

Parameters	Values
Mesh size (circum. × depth)	200×20
Journal diameter	53 [mm]
Bearing width	17 [mm]
Clearance	0.063 [mm]
Dynamic viscosity	$3.5 \cdot 10^{-2}$ [Pa·s]
Roughness	$5 \cdot 10^{-4}$ [mm]
Composite elastic modulus	206000 [MPa]
Elastic factor	$3 \cdot 10^{-3}$
Area moment of inertia of journal	387323 [mm^4]
Translational spring coefficient	$10 \cdot 10^{+7}$ [N/mm]
Rotational spring coefficient	$3.62 \cdot 10^{+5}$ [N·mm/rad]

Table 1 shows the simulation parameters used in the numerical model. Numerical results are compared with the experimental results of [17] at measured points to validate the model. Fig. 8 shows a pressure distribution which has a steep slope around the edge and a flat slope around the center. Generally, if the flexibility of the journal and bearing is not considered, the pressure distribution shows a parabolic shape along the depth direction as shown in the numerical results of rigid case in Fig. 8. But, because of the flexibility such as bending effect of journal or bearing, the pressure distribution becomes a flat shape around the center because the oil film thickness is increased in the center region. And a steep pressure distribution occurs around the edge and this can cause some wear phenomena which can be modeled as an asperity contact model. On the other hand, if we compare the numerical results with the experiment results, the pressure distribution around the edge of the experimental case is higher than that of the

numerical case and the pressure distribution around the center of the experimental case is lower than that of the numerical case. It may be that the bending effect of both journal and bearing is considered in the case of experiment result but the bending effect of journal is considered only in the numerical result. But, as shown in Fig. 8, the numerical results of current study show a good agreement with the experimental results and the numerical results of current study show much better solution than that of the rigid case.

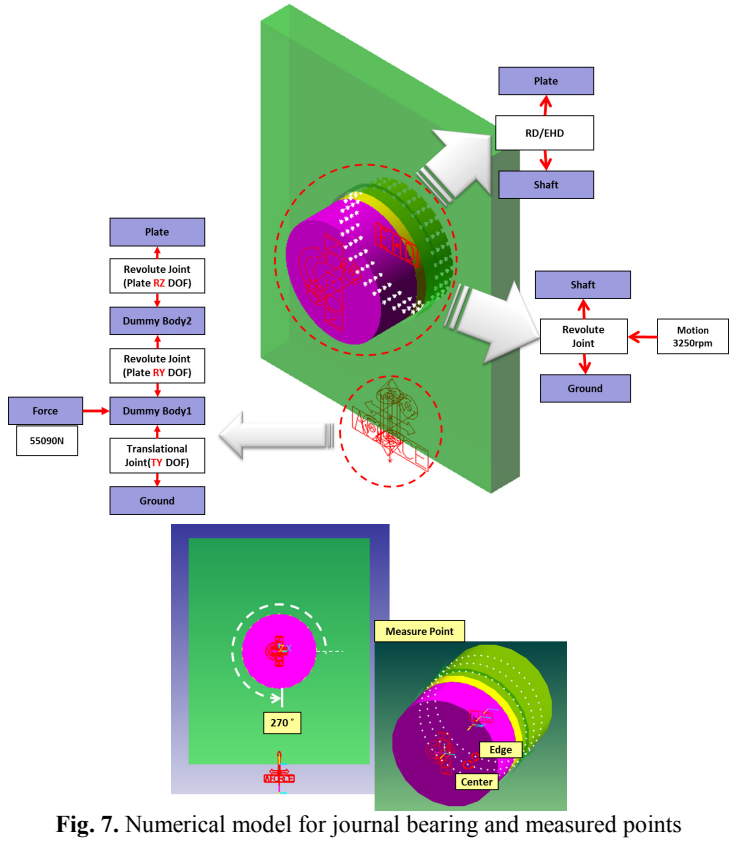

Fig. 7. Numerical model for journal bearing and measured points

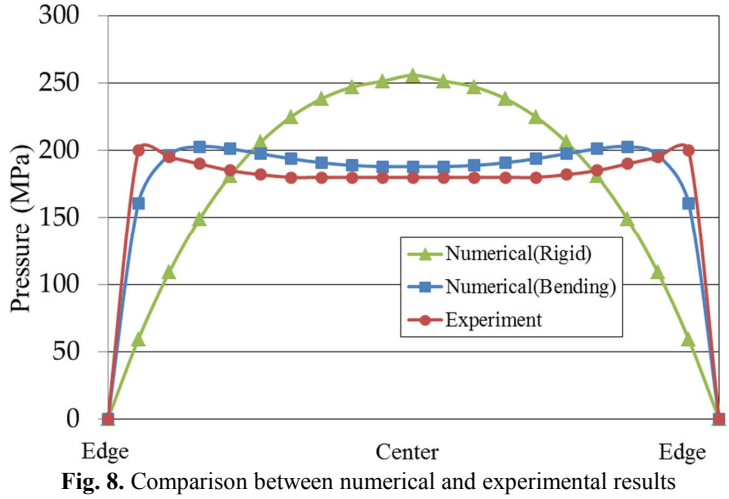

Fig. 8. Comparison between numerical and experimental results

7. Conclusions

In this study, the elastohydrodynamic lubrication analysis considering the bending effect of journal was coupled with multi-flexible-body dynamics (MFBD) to analyze dynamic bearing lubrication characteristics such as the pressure distribution and oil film thickness. To solve coupled fluid-structure interaction system, this study uses a MFBD solver and an EHD module iteratively. Especially, asperity contact model and bending stiffness effect model are introduced in EHD module. In the case of asperity contact model, the asperity contact pressure is calculated from the asperity contact model and then it is reflected on the oil film pressure. In the case of bending stiffness effect model, the oil film thickness is updated by using the bending stiffness effect model based on the beam theory. And then the updated oil film thickness is used to solve Reynolds equation. Additionally, functions such as mesh grid control and oil hole and groove effects are also implemented. Finally, the numerical results are validated and compared with the experimental results for the journal bearing example.

References

[1] **Taylor C. M.** Engine Tribology, Elsevier Science Publishers B. V., 1993, p.75-87.
[2] **Oh K. P., Goenka P. K.** The elastohydrodynamic solution of journal bearings under dynamic loading. ASME, Journal of Tribology, Vol. 107, No. 3, 1985, p. 389-395.
[3] **Labouff G. A., Booker J. F.** Dynamically loaded journal bearings: a finite element treatment for rigid and elastic surfaces. ASME, Journal of Tribology, Vol. 107, No. 4, 1985, p. 505-515.
[4] **Reynolds O.** On the theory of lubrication and its application to Mr. Beauchamp tower's experiments, including an experimental determination of the viscosity of olive oil. Phil. Trans. Roy. Soc., Vol. 177, 1886, p. 157-234.
[5] **Peiskammer D., Riener H., Prandstotter M., Steinbatz M.** Simulation of motor components: integration of EHD - MBS - FE - Fatigue. ADAMS User Conference, 2002.
[6] **Riener H., Prandstotter M., Witteveen W.** Conrod simulation: integration on EHD - MBS - FE – Fatigue. ADAMS User Conference, 2001.
[7] **Choi J.** A Study on the Analysis of Rigid and Flexible Body Dynamics with Contact. Ph. D. Dissertation, Seoul National University, Seoul, 2009.
[8] **Zhu D., Cheng H. S.** Effect of surface roughness on the point contact EHL. Trans. ASME, Journal of Tribology, Vol. 110, 1998, p. 32-37.
[9] **Greenwood J. A., Tripp J. H.** The contact of two nominally flat rough surfaces. Proc. Instn. Mech. Engrs., Vol. 185, Part 1, No. 48, 1971, p. 625-633.
[10] **Chung G., Hulbert G. M.** A time integration algorithm for structural dynamics with improved numerical dissipation: the generalized-α method. Trans. ASME, J. Applied Mechanics, Vol. 60, No. 2, 1993, p. 371-375.
[11] **Sabersky R. H., Acosta A. J., Hauptmann E. G.** Fluid Flow: A First Course in Fluid Mechanics. Third Edition, Maxwell Macmillan International Editions, 1989.
[12] **Gohar R.** Elastohydrodynamics. Second Edition, Imperial College Press, 2001.
[13] **Jang S., Park Y.** Study on the effect of aerated lubricant on the journal trace in the engine bearing clearance. International Journal of Automotive Technology, Vol. 6, No. 4, 2005, p. 421-427.
[14] **Patankar S. V.** Numerical Heat Transfer and Fluid Flow. Hemisphere, Washington, 1980.
[15] **Choi J., Kim S. S., Rhim S. S., Choi J. H.** Numerical modeling of journal bearing considering both elastohydrodynamic lubrication and multi-flexible-body dynamics. International Journal of Automotive Technology, Vol. 13, No. 2, 2012, p. 255-261.
[16] RecurDyn™ Manual. http://www.functionbay.co.kr, Function Bay, Inc., 2012.
[17] **Okamoto Y., Kitahara K., Ushijima K., Aoyama S., Jones G. J., Xu H.** Effects of the design parameters on wear and fatigue of engine bearings by EHL analysis. Seoul, 2000 FISITA World Automotive Congress, June 12-15, 2000.

